



CHORUS

This is the accepted manuscript made available via CHORUS. The article has been published as:

Measurement of the Femtosecond Optical Absorption of $\text{LaAlO}_3/\text{SrTiO}_3$ Heterostructures: Evidence for an Extremely Slow Electron Relaxation at the Interface

Yasuhiro Yamada, Hiroki K. Sato, Yasuyuki Hikita, Harold Y. Hwang, and Yoshihiko Kanemitsu

Phys. Rev. Lett. **111**, 047403 — Published 24 July 2013

DOI: [10.1103/PhysRevLett.111.047403](https://doi.org/10.1103/PhysRevLett.111.047403)

Femtosecond optical absorption measurements of LaAlO₃/SrTiO₃ heterostructures: Evidence for an extremely slow electron relaxation

Yasuhiro Yamada¹, Hiroki K. Sato^{2,3}, Yasuyuki Hikita², Harold Y. Hwang^{2,4}, and Yoshihiko Kanemitsu^{1,*}

¹*Institute for Chemical Research, Kyoto University, Uji, Kyoto 611-0011, Japan*

²*Stanford Institute for Materials and Energy Sciences, SLAC National Accelerator Laboratory, Menlo Park, California 94025, USA*

³*Department of Advanced Materials Science, The University of Tokyo, Kashiwa, Chiba, 277-8561, Japan*

⁴*Geballe Laboratory for Advanced Materials, Department of Applied Physics, Stanford University, Stanford, California 94305, USA*

Abstract

The photocarrier relaxation dynamics of an n-type LaAlO₃/SrTiO₃ heterointerface is investigated using femtosecond transient absorption (TA) spectroscopy at low temperatures. In both LaAlO₃/SrTiO₃ heterostructures and electron-doped SrTiO₃ bulk crystals, the TA spectrum shows a Drude-like free carrier absorption immediately after excitation. In addition, a broad absorption band gradually appears within 40 ps, which corresponds to the energy relaxation of photoexcited free electrons into self-trapped polaron states. We reveal that the polaron formation time is enhanced considerably at the LaAlO₃/SrTiO₃ heterointerface as compared to bulk crystals. Further, we discuss the interface effects on the electron relaxation dynamics in conjunction with the splitting of the t_{2g} subbands due to the interface potential.

PACS Numbers: 78.47.jb: 78.66.-w: 78.47.D-: 78.55.Hx:

* Corresponding author: kanemitsu@scf.kyoto-u.ac.jp

The interface between two insulating transition metal oxides can generate unique electronic systems [1]. These interfacial electronic systems have emerged as one of the most exciting areas in materials science and have potential use in the development of future oxide-based electronic devices. One striking example is the $\text{LaAlO}_3/\text{SrTiO}_3$ (LAO/STO) heterointerface; a quasi-two dimensional electron gas (2DEG) system confined to the depth of a few nanometers appears at this interface [2-10]. It has been demonstrated previously that the interface conductivity is sensitive to the electrostatic boundary conditions and that the $\text{LaAlO}_3/\text{TiO}_2$ interface exhibits n-type conduction [2-4]. The LAO/STO quasi-2DEG system exhibits very high sheet conductance and a variety of exotic phenomena such as two-dimensional superconductivity and magnetism [5,8-13]. Therefore, the LAO/STO system has been intensively investigated as a model oxide heterointerface. Accordingly, much effort has been devoted to reveal the unique electronic properties of such quasi-2DEG systems.

Recently, it has been found both theoretically and experimentally that the coexistence of localized and free carriers plays a critical role in the conduction mechanism at the LAO/STO heterointerface [14-16]. According to Ref. 15, localized electrons in a deep subband are confined within the first unit cell and have a low mobility due to Anderson localization and strong electron-phonon coupling. In contrast, high mobility free electrons above the lowest energy band spread over several Ti layers. The categorization of carriers into two different types is essential for understanding the LAO/STO interface conductivity. On the other hand, carriers in SrTiO_3 bulk crystals are also considered to have a localized nature, which has been discussed in terms of defect/impurity states and polarons, which are self-trapped states resulting from strong electron-phonon coupling [17-19]. For example, photoemission spectroscopy in lightly electron-doped or photoexcited SrTiO_3 suggests the coexistence of localized and free electrons [20,21]. Further, we recently reported that the photoluminescence (PL) spectrum of SrTiO_3 has both a sharp band edge peak and a broad band with a large

Stokes shift at low temperatures [22], indicating the coexistence of free carriers in band states and localized photocarriers in trapped states. These observations imply that polaronic carrier localization mechanisms might be the key factors that determine the electronic properties of SrTiO₃ and SrTiO₃-based heterostructures. Thus, it is essential to reveal the energy relaxation processes of carriers at the SrTiO₃ heterointerface.

In this letter, we report the relaxation dynamics of electrons in an n-type LAO/STO heterointerface and compare this interface to bulk SrTiO₃ crystals by using femtosecond transient absorption (TA) measurements. In bulk SrTiO₃, the photoexcited electrons relax into self-trapped states within several tens of picoseconds. We found an extremely reduced relaxation rate, in comparison, of photoexcited electrons at the LAO/STO heterointerface, which could be attributed to the splitting of t_{2g} subbands at the LAO/STO interface. Our results provide deep insight into the physics behind the electronic properties of oxide interfaces and promote the understanding of interface conduction mechanisms.

We used chemically electron-doped SrTiO₃ single crystals [SrNb_xTi_{1-x}O₃ (x=0.001): Nb-STO] (Furuuchi Chemical Co.), Ar⁺-irradiated SrTiO₃ (Ar-STO; the fabrication method and spatial profile of the carrier density are described in Ref. 23), and n-type LAO/STO heterostructures. The LAO/STO interfaces were grown by pulsed laser deposition using a single crystal LaAlO₃ target on TiO₂-terminated (001) SrTiO₃ single crystal substrates after the deposition of a SrTiO₃ buffer layer (10 unit cells). The (LaO)⁺/(TiO₂)⁰ interface was grown by direct deposition on this surface using a KrF excimer laser at a repetition rate of 4 Hz and a laser fluence of 1.2 Jcm⁻² at the target surface. For SrTiO₃ buffer layer and LaAlO₃ overlayer growth, the growth temperature was 700°C with an oxygen partial pressure $p_{O_2} = 1 \times 10^{-5}$ Torr. The LaAlO₃ overlayer thickness was 32 unit cells. We confirmed the existence of metallic interface conduction in the heterostructure. PL spectra were collected using a CCD camera with a monochromator. The light source was a wavelength tunable Yb:KGW-based

femtosecond laser system (pulse width: 290 fs, repetition rate: 200 kHz). The TA measurements were performed by a standard pump-probe technique using a Yb:KGW laser system, where the fundamental light (1.20 eV) was used as a probe pulse. The pump and probe pulses were focused on the sample surface, and we detected the TA signal, the variation of the probe pulse intensity induced by the pump photoexcitation. To measure the probe energy dependence of TA dynamics, we used a Ti:sapphire-based femtosecond laser (pulse width: 150 fs, repetition rate: 1 kHz) with two optical parametric amplifiers. The laser spot size on the sample surface was measured using the knife-edge method.

First, we studied the PL spectra of a LAO/STO heterostructure to identify and discuss interface effects on the photocarrier recombination process. Figure 1(a) shows the PL spectrum of the LAO/STO heterostructure at 7 K. The excitation photon energy was 3.82 eV, corresponding to a penetration depth $\lambda_p = 25$ nm [23]. The PL spectrum of LAO/STO is qualitatively identical to that of chemically electron-doped SrTiO₃ bulk crystals. The PL spectrum is composed of a sharp band edge PL peak and a broad green PL band [22, 24]. The large Stokes shift of the broad PL band indicates that the PL process involves strongly localized states, which have previously been assigned to impurity/defect states or self-trapped states (polarons) [24,25]. The sharp band edge PL corresponds to band-to-band recombination of free electrons at the conduction band and free holes in the valence band [22]. Figs. 1(c) and (d) show the PL spectra near the band gap energy of the LAO/STO heterostructure and Nb-STO under an excitation of 3.82 eV ($\lambda_p = 25$ nm) and 3.49 eV ($\lambda_p = 240$ nm). According to the penetration depth λ_p , the PL spectrum under 3.82 eV excitation reflects the surface (interface) state of SrTiO₃, while 3.49 eV excitation light probes the interior state of the SrTiO₃ bulk crystals (see schematic picture shown in Fig. 1(b)). This observation then implies that the nature of carriers at the LAO/STO interface and electron-doped SrTiO₃ bulk crystals are similar.

To determine the relaxation dynamics of photocarriers, we performed TA spectroscopy at low temperatures. It is known that electron-doped or photoexcited SrTiO₃ exhibits a broad optical absorption band in the infrared region [26-28]. The TA signal is observed under excitation at an energy above the band gap. We confirmed that this broad absorption band originates from electron photo-absorption by comparing the TA and photoconductance dynamics.

Figure 2 (a) shows the TA dynamics of Nb-doped SrTiO₃ at 7 K under different probe energies. The pump energy was 3.5 eV. The longitudinal axis represents the transmittance reduction of the probe pulse induced by pump pulse excitation, $-\Delta T/T$. We checked whether the TA dynamics was independent of excitation density and polarization direction of the pump and probe pulses. The TA profile is composed of two components. One component represents fast decay with an exponential decay time of about 1 ps, as shown in Fig. 2(b). We attribute the fast decaying component to the relaxation to the conduction band minimum of higher energy photoexcited electrons (intra-band relaxation). This interpretation is supported by the fact that the relative intensity of the fast decay component decreases with decreasing excitation energy [see Fig. 3]. The second component of the TA profile shows a gradual rise with a rise time of about 40 ps at probe energies above 1.0 eV. This component decreases at a lower probe energy (<1.0 eV). The TA dynamics between 5 and 300 ps is well reproduced by a single exponential function, as shown by the broken curves in Fig. 2(a). The rise/decay time is 40 ps, independent of the probe energy.

To investigate the origin of the second component with a 40 ps rise time, we plotted the TA spectrum (probe energy dependence of the TA signal intensity) at 5 ps and 300 ps in Fig. 2(c). At 5 ps, a time much longer than the intra-band relaxation time, the TA spectrum shows Drude-like dispersion (ω^{-2} , as shown by the blue broken curve), which indicates that the electrons are in free states. On the other hand, the TA spectrum becomes non-Drude-like at

300 ps and a broad absorption band appears at around 1.5 eV. This broad absorption band corresponds to the transition from a localized state to a free carrier state. As schematically shown in Fig. 2(d), photo-generated electrons immediately relax to the bottom of the conduction band and the TA shows a Drude-like free carrier absorption [denoted by X in Fig. 2(d)]. When the electrons fall into a localized state, the TA contribution of the transition from a localized state to a free conduction band state appears [denoted by Y]. These results suggest that some parts of the photoexcited electrons are localized at 300 ps. Therefore, we can conclude that the 40 ps rise/decay component corresponds to the relaxation process of free electrons into localized states.

Here, we consider the origin of the observed localized state. One possibility is the presence of shallow trap states due to defects or impurities. However, trap levels in electron-doped SrTiO₃ should be fully occupied at low temperatures, and therefore, no TA contribution from the trap levels appears. In addition, we confirmed that the TA signal intensity linearly increases with increasing excitation intensity in the range of 0.12–2.2 mJ/cm². If the TA signal has contributions from finite number of defects/impurities, the excitation density dependence of the TA intensity should saturate. Therefore, we can conclude that no defects/impurities contribute to the TA signals. Instead, we consider that polarons are the most likely origin for such localized states in SrTiO₃ bulk crystals. In SrTiO₃, electrons are self-trapped by accompanying lattice distortions due to strong electron-phonon coupling [18,25]. Because the polaron density of states is much higher than that of defect/impurity states, photoexcited electrons are self-trapped even in electron-doped SrTiO₃. In this case, the rise/decay time corresponds to the polaron formation time in the electron-doped SrTiO₃ bulk crystal.

To compare the polaron formation dynamics in electron-doped SrTiO₃ bulk crystals and at the LAO/STO interface, we studied the pump energy dependence of the TA dynamics because

the photon energy is strongly dependent on the penetration depth of the incident light. Figure 3 shows TA dynamics in (a) Nb-STO (−30~310 ps) and (b) LAO/STO heterostructures (−100~1200 ps) under different excitation energies. The probe photon energy was fixed at 1.2 eV. Nb-STO shows a gradual increase in TA intensity with a rise time of several tens of picoseconds, similar to undoped SrTiO₃. The TA dynamics is well reproduced by a single exponential function between 5 ps and 300 ps. The intensity of the fast decaying component increases with excitation energy due to intra-band relaxation of photoexcited electrons. On the other hand, the fast and slow TA relaxation times are almost independent of excitation photon energy. This observation implies that the relaxation dynamics into the polaron state is independent of excitation energy in spatially homogeneous SrTiO₃ crystals.

In LAO/STO heterostructures, the TA signal under an excitation of 3.35 eV, which probes the interior state of the SrTiO₃ substrate, also shows a gradual increase of about 40 ps in lifetime. On the other hand, under an excitation of 3.88 eV, which corresponds to the first 20 nm of the penetration depth, the polaron formation time is extremely elongated and reaches about 600 ps. This result clearly indicates that a slowing down of polaron formation occurs at the LAO/STO interface as compared to that for bulk crystals. It should be noted that the TA rise component under high energy excitation shows a non-single-exponential profile, unlike in the case of Nb-STO. This difference is probably due to the spatial inhomogeneity of the carrier density and potential near the LAO/STO heterointerface [29]. Thus, to evaluate the observed TA profile that is not a single-exponential profile, we fitted the TA curves with a double exponential function $I_{TA}(t) = A_1 \exp(-t/\tau_1) + A_2 \exp(-t/\tau_2)$ between 5 and 1200 ps and defined the relaxation time as $\langle \tau \rangle = (A_1 \tau_1 + A_2 \tau_2) / (A_1 + A_2)$.

Figure 4(a) summarizes the relaxation times of Nb-STO, Ar-STO, and LAO/STO heterostructures as a function of penetration depth. The relaxation time of the LAO/STO heterostructure shows a sudden increase for pump energies above 3.75 eV (penetration depth

= 30 nm) [30]. This increase implies that polaron formation is strongly suppressed at the LAO/STO heterointerface. To eliminate the possibility that oxygen vacancies induced at the heterointerface affect the polaron formation time, we studied the relaxation times of Ar-STO, where oxygen vacancies are formed at the surface by Ar⁺ irradiation. As shown in Fig. 4(a), the relaxation time of Ar-STO is almost independent of the penetration depth and is similar to that of Nb-STO. These results clearly demonstrate that oxygen vacancies do not affect the carrier localization process and the LAO/STO heterointerface plays an essential role for the suppression of polaron formation. Interestingly, in both Nb-STO and Ar-STO bulk crystals, the relaxation time becomes slightly longer with a decrease in penetration depth. This suggests that the weak suppression of polaron formation may occur even at the surface of SrTiO₃.

Finally, we discuss the slow relaxation of photoexcited electrons into localized states at the LAO/STO heterointerface. At the heterointerface, band bending occurs (schematically shown in Fig. 4(b)), which strongly affects the polaron formation process. One possible mechanism that causes slow polaron formation dynamics is related to the splitting of Ti 3*d* levels due to a strong interface potential. In SrTiO₃, the lowest energy conduction band is composed of *t*_{2g} orbitals of Ti 3*d* states, which are degenerate at the Γ point at temperatures above 105 K (cubic-to-tetragonal structural phase transition in bulk crystals). At low temperatures below 105 K, the weak energy splitting of *t*_{2g} levels occurs due to tetragonal distortions [31]. Furthermore, for the LAO/STO heterointerface, the interface potential causes a larger energy splitting of the *t*_{2g} level [14,32], as schematically shown in Fig. 4(c). The lowest energy *d*_{xy}-like subband has an extremely large electron effective mass in the *z* direction, and thus, electrons can be self-trapped due to phonon couplings in this subband [33]. Therefore, the photoexcited carriers relax into the polaron state through the lowest-energy *d*_{xy}-like subband. In this case, the polaron formation time is determined by the transition rate

from other subbands to the lowest-energy subbands. Because the energy splitting at the interface is much larger than that for bulk crystals, the transition rate is correspondingly reduced at the heterointerface. In addition, the photoexcited electrons are driven by the strong electric field from the large band bending at the interface, which can prevent the relaxation of photocarriers into polaron states.

Despite the longer polaron formation time, the electron mobility is not correspondingly enhanced at the heterointerface, because the electrons at equilibrium are concentrated to the lowest-energy subband due to the large energy splitting at the LAO/STO heterointerface. This scenario is consistent with the ratio of the non-Drude component in the TA curve at the LAO/STO heterointerface. As shown in Fig. 3(b), the gradually rising component is dominant in the TA dynamics at the LAO/STO heterointerface (excited at 3.88 eV), indicating that the non-Drude TA component is much larger than the Drude component. This indicates that most of the photoexcited electrons at the heterointerface relax into localized polaron states, which would suppress the electron mobility.

In this work, we studied the relaxation dynamics of free electrons into polaron states in SrTiO₃ bulk crystals and n-type LAO/STO heterostructures. On the basis of the TA dynamics measurements, we estimated the carrier relaxation time at low temperatures and revealed that polaron formation is strongly suppressed at the LAO/STO heterointerface, unlike SrTiO₃ bulk crystals. We discussed the slowing down of the time required for polaron formation in quasi-2DEG systems in conjunction with the t_{2g} energy splitting due to the strong electric field at the interface. Our results should provide important insights into the unique electronic conduction mechanisms of oxide interfaces.

References

- [1] H. Y. Hwang, Y. Iwasa, M. Kawasaki, B. Keimer, N. Nagaosa, and Y. Tokura, *Nat. Mater.* **11**, 103 (2012).
- [2] A. Ohtomo and H. Y. Hwang, *Nature (London)* **427**, 423 (2004).
- [3] N. Nakagawa, H. Y. Hwang, and D. A. Müller, *Nature Mater.* **5**, 204 (2006).
- [4] S. Thiel, G. Hammerl, A. Schmehl, C. W. Schneider, J. Mannhart, *Science* **313**, 1942 (2006).
- [5] N. Reyren, S. Thiel, A. D. Caviglia, L. Koukoutis, G. Hammerl, C. Richter, C. W. Schneider, T. Kopp, A. S. Rüetschi, D. Jaccard, M. Gabay, D.A. Muller, J. M. Triscone, and J. Mannhart, *Science* **317**, 1196 (2007).
- [6] M. Basletic, J.-L. Maurice, C. Carrétéro, G. Herranz, O. Copie, M. Bibes, É. Jacquet, K. Bouzehouane, S. Fusil, and A. Barthélémy, *Nat. Mater.* **7**, 621 (2008).
- [7] K. Janicka, J. P. Velev, and E. Y. Tsymlal. *Phys. Rev. Lett.* **102**, 106803(2009).
- [8] A. D. Caviglia, S. Gariglio, C. Cancellieri, B. Sacépé, A. Fête, N. Reyren, M. Gabay, A. F. Morpurgo, and J.-M. Triscone, *Phys. Rev. Lett.* **105**, 236802 (2010).
- [9] R. Yamamoto, C. Bell, Y. Hikita, H. Y. Hwang, H. Nakamura, T. Kimura, and Y. Wakabayashi, *Phys. Rev. Lett.* **107**, 036104 (2011).
- [10] J. A. Bert, K. C. Nowack, B. Kalisky, H. Noad, J. R. Kirtley, C. Bell, H. K. Sato, M. Hosoda, Y. Hikita, H. Y. Hwang, and K. A. Moler, *Phys. Rev. B* **86**, 060503(R) (2012).
- [11] A. Brinkman, M. Huijben, M. van Zalk, J. Huijben, U. Zeitler, J. C. Maan, W. G. van der Wiel, G. Rijnders, D. H. Blank, and H. Hilgenkamp, *Nat. Mater.* **6**, 493 (2007).
- [12] J. A. Bert, B. Kalisky, C. Bell, M. Kim, Y. Hikita, H. Y. Hwang, and K. A. Moler, *Nat. Phys.* **7**, 767 (2011).
- [13] L. Li, C. Richter, J. Mannhart, and R. C. Ashoori, *Nat. Phys.* **7**, 762 (2011).

- [14] Z. S. Popovic, S. Satpathy, and R. M. Martin, Phys. Rev. Lett. **101**, 256801 (2008).
- [15] T. Fix, F. Schoofs, J. L. MacManus-Driscoll, and M. G. Blamire, Phys. Rev. Lett. **103**, 166802 (2009).
- [16] K.-J. Zhou, M. Radovic, J. Achlappa, V. Strocov, R. Frison, J. Mesot, L. Patthey, and T. Schmitt, Phys. Rev B **83**, 201402(R) (2011).
- [17] O. Bidault, M. Maglione, M. Actis, M. Kchikech, B. Salce, Phys. Rev. B **52**, 4191 (1995).
- [18] D. Keroack, Y. Lepine and J. L. Brebner, J. Phys. C: Solid State Phys. **17**, 833(1984).
- [19] J. T. Devreese, S. N. Klimin, J. L. M. van Mechelen, and D. van der Marel, Phys. Rev. B **81**, 125119 (2010).
- [20] Y. Ishida, R. Eguchi, M. Matsunami, K. Horiba, M. Taguchi, A. Chainani, Y. Senba, H. Ohashi, H. Ohta, and S. Shin, Phys. Rev. Lett. **100**, 056401 (2008).
- [21] T. Mizokawa, N. Takaiwa, Y. Fujiwara, T. Iida, J.-Y. Son, T. Ishikawa, M. Itoh, and M. Takesada, J. Phys. Soc. Jpn. **79**, 044703 (2010).
- [22] Y. Yamada and Y. Kanemitsu Phys. Rev. B **82**, 121103(R) (2010).
- [23] H. Yasuda, Y. Yamada, T. Tayagaki, and Y. Kanemitsu, Phys. Rev. B **78**, 233202 (2008).
- [24] Y. Yamada, H. Yasuda, T. Tayagaki, and Y. Kanemitsu, Phys. Rev. Lett. **102**, 247401 (2009).
- [25] T. Hasegawa, M. Shirai, and K. Tanaka, J. Lumin. **87-89**, 1217 (2000).
- [26] H. Okamura, M. Matsubara, K. Tanaka, K. Fukui, M. Terakami, H. Nakagawa, Y. Ikemoto, T. Moriwaki, H. Kimura, and T. Nanba, J. Phys. Soc. Jpn. **75**, 023703 (2006).
- [27] J. L. M. van Mechelen, D. van der Marel, C. Grimaldi, A. B. Kuzmenko, N. P. Armitage, N. Reyren, H. Hagemann, I. I. Mazin, Phys. Rev. Lett. **100**, 226403 (2008).
- [28] Y. Yamada, H. Yasuda, T. Tayagaki, and Y. Kanemitsu, Appl. Phys. Lett. **95**, 121112 (2009).

[29] We tuned the probe area by changing the penetration depth (or photon energy) of the incident pump pulse. Therefore, the observed TA signal at the LAO/STO heterointerface was the sum of various exponential functions with different relaxation times, because the TA relaxation time of LAO/STO was quite sensitive to the depth from the interface, as indicated by our experimental results.

[30] The observed TA signal intensity is integrated over the photoexcited volume. Therefore, even in the case of 100-nm penetration depth, the TA signal still has a dominant contribution from the LAO/STO interface. The large rise time at around 100-nm penetration depth shown in Fig. 4(a) does not suggest that the LAO/STO interface has widespread effects to 100 nm in depth.

[31] R. Bistritzer, G. Khalsa, and A. H. MacDonald, *Phys. Rev. B* **83**, 115114 (2011).

[32] M. Salluzzo, J. C. Cezar, N. B. Brookes, V. Bisogni, G. M. De Luca, C. Richter, S. Thiel, J. Mannhart, M. Huijben, A. Brinkman, G. Rijnders, and G. Ghiringhelli, *Phys. Rev. Lett.* **102**, 166804 (2009).

[33] A. F. Santander-Syro, O. Copie, T. Kondo, F. Fortuna, S. Pailhes, R. Weht, X. G. Qiu, F. Bertran, A. Nicolaou, A. Taleb-Ibrahimi, P. Le Fevre, G. Herranz, M. Bibes, N. Reyren, Y. Apertet, P. Lecoeur, A. Barthelemy, and M. J. Rozenberg, *Nature (London)* **469**, 189 (2011).

Figure 1 (Color online)

(a) PL spectrum of LAO/STO heterostructure at 7 K under an excitation of 3.82 eV. The PL intensity above 3.0 eV is expanded. (b) Schematic picture of the penetration depth for excitation light at 3.82 eV and 3.49 eV. (c)(d) PL spectra of LAO/STO heterostructures and Nb-STO crystals near the band gap energy at 7 K under an excitation of 3.82 and 3.49 eV.

Figure 2 (Color online)

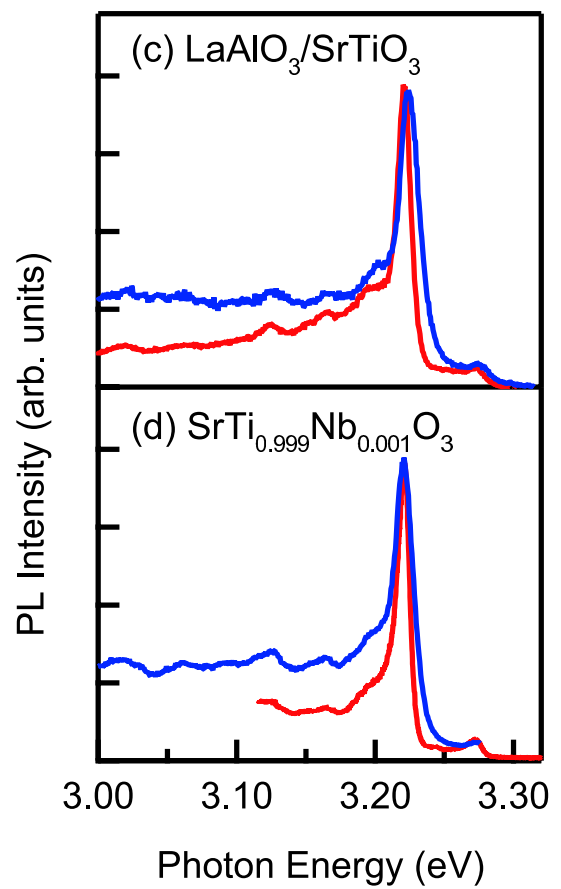
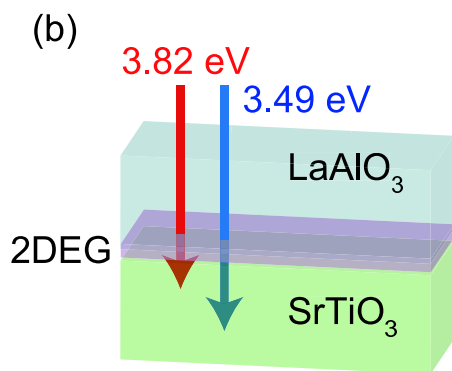
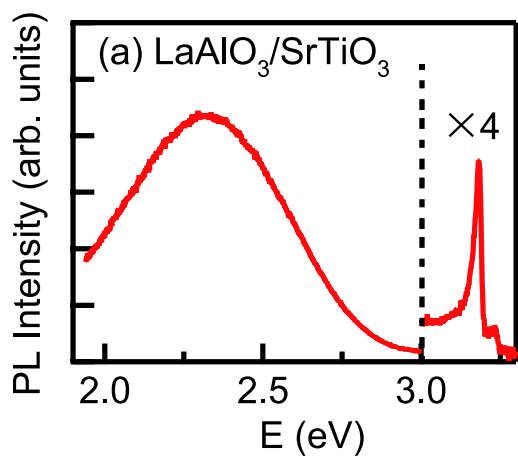
(a) TA dynamics of Nb-STO at 7 K under different probe energies. The dotted curves show the exponential fitting results with a relaxation time of 40 ps. (b) Enlarged view of the TA dynamics in the range of 3~13 ps at a probe energy of 1.38 eV. (c) TA spectra monitored at 5 ps and 300 ps. The dotted lines for TA at 5 ps and 300 ps are the fitted curves for a simple Drude dispersion (ω^{-2}) and Drude dispersion added with a Gaussian function, respectively. (d) Band diagram and TA processes in SrTiO₃. Red arrows correspond to (X) free carrier absorption and (Y) transition from localized states to the free conduction band state. The blue broken arrow refers to the energy relaxation of electrons into localized states.

Figure 3 (Color online)

TA dynamics of (a) Nb-STO and (b) LAO/STO heterostructures at 7 K under an excitation of 3.88, 3.65, and 3.35 eV. The solid curves correspond to fits of a single exponential function in Nb-STO and a double exponential function in LAO/STO heterostructures.

Figure 4 (Color online)

(a) Electron relaxation times of Nb-STO, Ar-STO, and LAO/STO heterostructures as a function of the penetration depth of the excitation light. (b) Schematic band diagram at the LAO/STO heterointerface and the penetration depth for excitation light at 3.88 eV and 3.35 eV. (c) Schematic graph of the energy diagram of t_{2g} levels of Ti 3d orbitals.



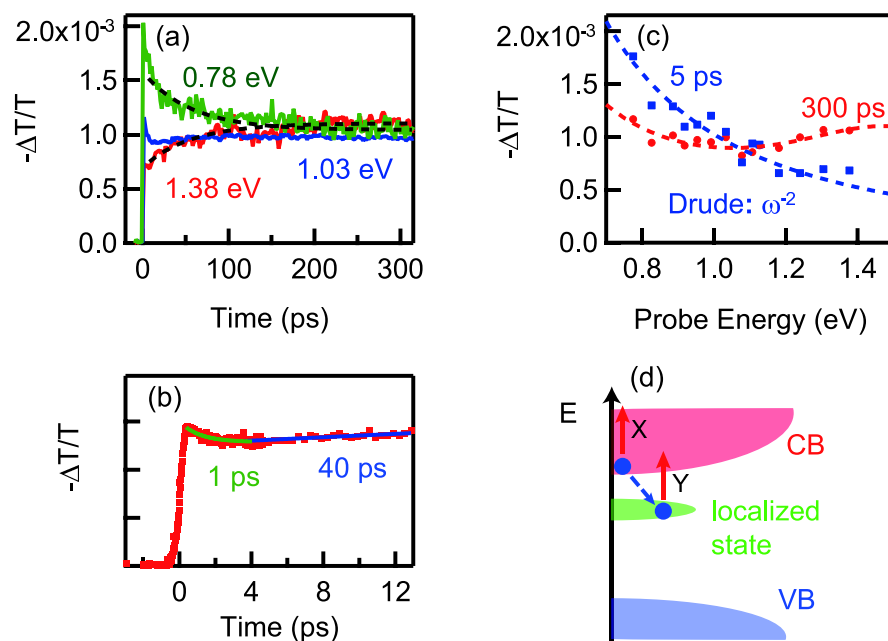


Figure 2

LA13643

28MAY2013

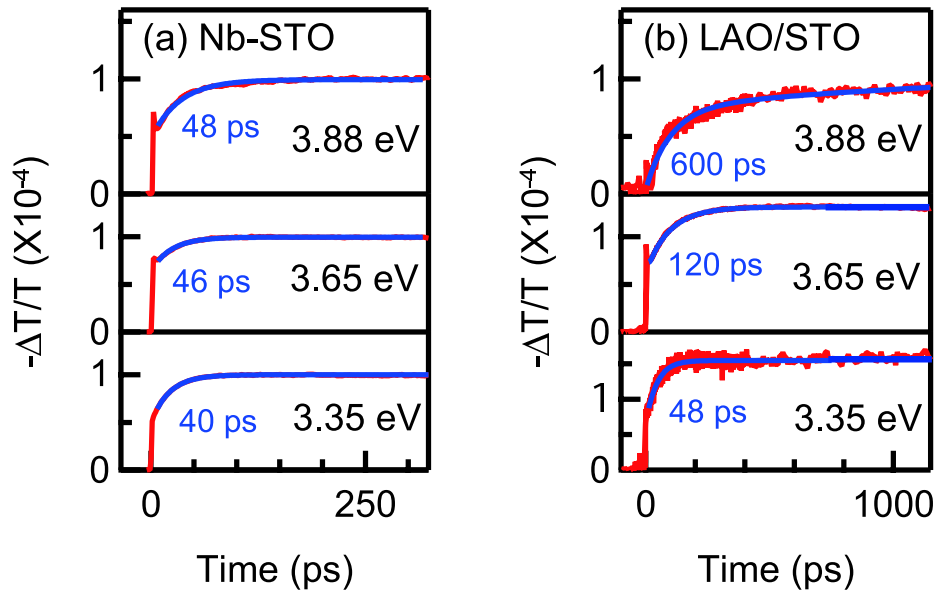


Figure 3

LA13643

28MAY2013

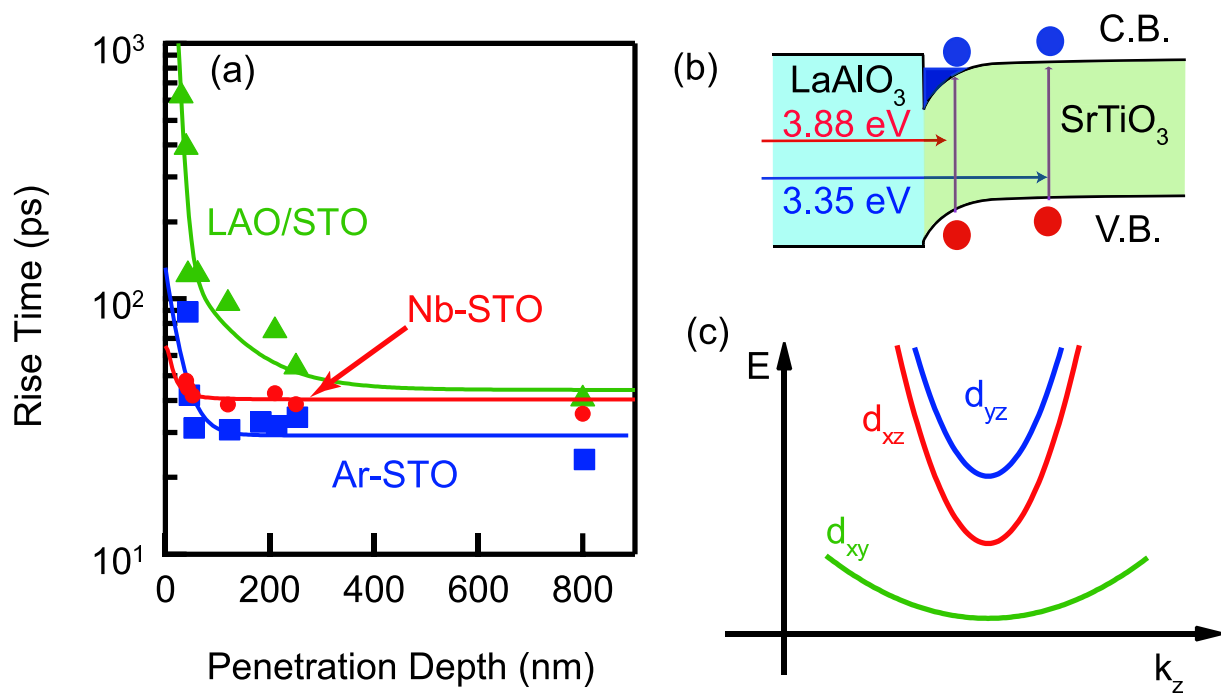


Figure 4 LA13643 28MAY2013